

# Eigenfunction and eigenmode-spacing statistics in chaotic photonic crystal graphs

Shukai Ma,<sup>1,\*</sup> Thomas M. Antonsen,<sup>2,3</sup> Edward Ott,<sup>2,3</sup> and Steven M. Anlage<sup>1,3</sup>

<sup>1</sup>*Quantum Materials Center, Department of Physics,  
University of Maryland, College Park, Maryland 20742, USA*

<sup>2</sup>*Department of Physics, University of Maryland,  
College Park, Maryland 20742, USA*

<sup>3</sup>*Department of Electrical and Computer Engineering,  
University of Maryland, College Park, Maryland 20742-3285, USA*

## Abstract

The statistical properties of wave chaotic systems [of varying dimensionalities](#) have been studied extensively. [These systems are commonly characterized by the statistics of the](#) short-range and long-range eigenmode-spacing, and the one-point and two-point eigenfunction correlations. Here, we propose photonic crystal (PC) defect waveguide graphs as an alternative physical system for chaotic graph studies. Experimental studies of chaotic graph eigenfunctions have generally been confined to the wavefunction values at the nodes of the graph, because the graphs are usually constructed with coaxial cables that prevent [direct](#) access to the wave functions on the bonds. Recent studies reveal that chaotic graphs possess non-universal properties, which may be better analyzed and understood through eigenfunction analysis. Photonic crystal graphs have two novel features, namely an unusual dispersion relation for the propagating modes, and complex scattering properties of the junctions and bends. [Here we present numerically determined properties of](#) an ensemble of such PC-graphs [including](#) both eigenfunction amplitude and eigenmode-spacing studies. Our proposed system [is amenable](#) to other statistical studies, and may be realized experimentally.

## I. INTRODUCTION

Wave-chaotic phenomena have been studied in various systems, ranging from 1D graphs [1–4], 2D billiards [5–11] to 3D enclosures [12–17]. The statistical properties of many system quantities, such as the closed system eigenvalues and the open system scattering/impedance matrices, exhibit universal characteristics, which only depend on general symmetries (e.g., time-reversal, symplectic) and the system loss factors. The Random Coupling Model (RCM) has found great success in characterizing the statistical properties of a variety of experimental systems by removing the non-universal effects induced by port coupling and short-orbit effects [8, 12, 13, 15, 16, 18–23]. Chaotic microwave graphs support complex scattering phenomena despite their relatively simple structures, and allow for various useful circuit components (such as phase shifters and attenuators) to be incorporated into the structure [2–4]. Recent studies show that non-universal statistical features exist in chaotic graph systems, which is caused by the finite reflection at the graph vertices. These reflections create trapped modes that pollute the spectral statistics of the graph [3, 24–26]. However, the experimental investigation of such phenomena is complicated by the fact that only the node information is accessible from cable graph systems, which are the common choice for conducting graph experiments.

Here, we introduce an alternative type of chaotic graph built with photonic crystal (PC) systems. The PC graph bonds are realized with defect waveguides and the nodes are formed by the waveguide junctions. The electromagnetic waves propagating in the graph bonds are more accessible. With numerical simulation tools, we conduct a series of statistical tests of the photonic crystal graph system including both eigenvalue and eigenfunction studies of closed graphs. To our knowledge, PC graphs have not been previously utilized for chaotic

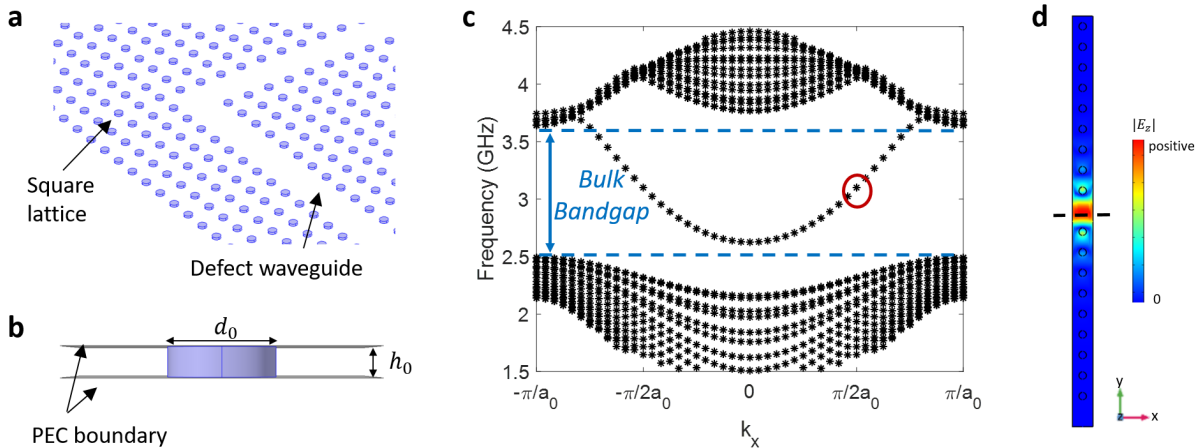


FIG. 1. **a.** The open-plate view of the photonic crystal lattice with an L-shaped defect waveguide region. **b.** The side view of the PC unit cell. A dielectric rod is sandwiched between two PEC (perfect electric conductor) surfaces. The quantities  $h_0$  and  $d_0$  are the height and diameter of the rod. **c.** The photonic band structure from a supercell defect waveguide simulation. The waveguide modes appear in the bulk bandgap region (blue dashed lines). **d.** The E-field profile of one of the waveguide mode solution (the red circle in **c**). The black dashed line marks the center of the waveguide.

graph studies.

The paper is organized as follows. In Section II, we introduce the design details of the proposed PC graph structure as well as its numerical implementation methods. We present the closed-graph mode-spacing study in section III, and focus on the discussion of closed-graph eigenfunction studies in section IV. Different methods of conducting eigenfunction statistical studies are also discussed. We summarize the paper and discuss the future applications of the proposed PC graphs in section V.

## II. PHOTONIC CRYSTAL GRAPH

A photonic crystal system consists of a regular lattice of artificial atoms (or scatterers) whose spacing is comparable to the operating wavelength [27, 28]. The material properties and the geometrical details of the atom are carefully designed in order to achieve a specific

functionality. A PC system is usually constructed as a 2D planar structure, which makes it especially good for photonics applications. Importantly, a 2D PC can show a complete bulk bandgap in its excitation spectrum [27, 28]. In PC-based devices, waveguides and cavities can be constructed for example by making air defects (removing a certain number of the atoms) in the original lattice. This creates guided propagating modes in the bulk bandgap, which ensures that the modes are confined to the defect region. [A variety of defect waveguides can be realized by changing the atom properties \[27\].](#) Recent photonic topological insulator studies present an alternative form of PC waveguide using a kinky interface between two different topological domains [29–33]. Bulk PC systems have also been employed to construct chaotic billiard systems [11, 34]. Here, we will utilize the defect waveguide modes to build chaotic graph structures.

The construction of the chaotic PC graph starts by building a square lattice with identical dielectric rods (the blue lattice in Fig. 1a). The lattice constant is  $a_0 = 36.8mm$ . The dielectric rod lattice is sandwiched between two metallic surfaces and installed in a vacuum background. The defect waveguide is created by simply taking out one row or column of the dielectric rods. The detailed shape of the dielectric rod is shown in Fig. 1b. The diameter of the dielectric rod is  $d_0 = 13.2mm$  and the height is  $h_0 = 0.1a_0 = 3.68mm$ . Because the PC lattice is thin in the vertical direction ( $z$ -direction), the waveguide modes considered here are transverse magnetic (TM) polarized ( $E_z \neq 0$ ,  $E_{x,y} = 0$ ,  $H_z = 0$  and  $H_{x,y} \neq 0$ ). The relative permittivity and permeability of the dielectric rods are  $\epsilon_r = 11.56$  and  $\mu_r = 1$ . We realize the proposed PC structure numerically with COMSOL Multiphysics Software. The presence of the waveguide mode is clearly demonstrated by the supercell photonic band structure (PBS) simulation (Fig. 1c). The supercell simulation model consists of a single column of PC lattice with Floquet periodic boundaries on the two long sides. The two short-

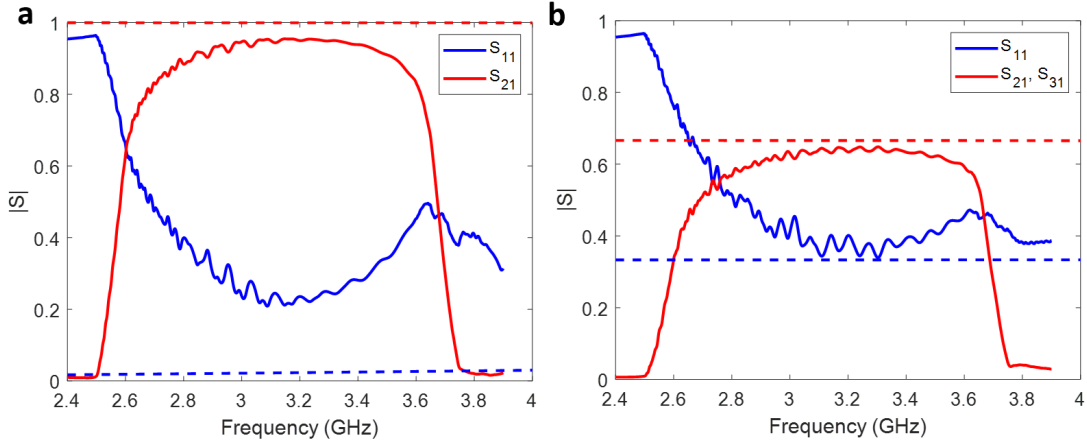


FIG. 2. **a.** The simulated S-parameters of the PC-graph right-angle L-junction (solid), as well as the S-parameter from a coaxial cable 3-port connector (dashed), which serves as a reference. **b.** The simulated S-parameters of the PC-graph T-junction (solid) and the S-parameters from a coaxial cable 3-port connector (dashed). All PC-junction S-parameters are frequency averaged with a 500MHz window to remove the effect of spurious reflections.

end surfaces are assigned totally absorbing boundary condition. We remove the center rod to create the defect waveguide region. The PBS simulation is conducted by computing the system eigenmodes while varying the wavenumber  $k_x$  in the range  $[-\pi/a_0, \pi/a_0]$ . As shown in Fig. 1c, the defect waveguide modes have emerged inside of the bulk bandgap region from 2.5 ~ 3.6GHz. Here we see the first unique feature of PC graphs – the PC waveguide modes present a more complicated dispersion relationship between  $\omega$  and  $k_x$  (e.g., modes near 2.6GHz in Fig. 1c) as compared with coaxial cable ( $\omega = ck_x$ ). In Fig. 1d, the  $|E_z|$  profile of the entire simulation domain shows clearly that the mode solution is indeed a guided wave because its amplitude is highly localized in the defect region.

The PC graph structure is realized by connecting multiple defect waveguides with both right-angle and T-shaped junctions. We have characterized the scattering matrix of both types of the junctions with COMSOL and CST Microwave STUDIO. For the right-angle bends, non-zero transmission is found only in the bulk bandgap region. As shown in Fig. 2a, The transmission values vary systematically near but below 1 as a function of frequency,

which qualifies the right-angle bends as vertices with a non-trivial scattering matrix in a graph. The PC-graph T-junction presents a complex scattering profile over the entire bandgap region. As shown in Fig. 2b, the magnitude of the reflection (transmission) coefficient deviates systematically from  $1/3$  ( $2/3$ ) as a function of frequency. These nontrivial scattering parameters are a second unique feature of PC graphs, and [can be expected to influence the properties of the graph eigenmodes](#). We note that alternative methods of making waveguide bends or connecting waveguides can be applied, for example by removing or adding dielectric rods at the right-angle turn, in order to tune the transmission property of the waveguide joints [35]. The engineering of the node transmission property is beyond the scope of this paper.

We simulate the closed PC graphs with the COMSOL eigenvalue solver. The PC graph system is drawn and sandwiched between two [metallic surfaces \(PEC boundaries\)](#). The graph topology is that of a flattened tetrahedral graph having 14 straight segments and 13 junctions (including 3-way junctions and right-angle bends). The four exterior faces of the PC structure are assigned totally absorbing boundary conditions. The total length of the simulated graph is on the scale of  $\sim 9m$ , which hosts about 80 eigenmodes (within the bulk PC bandgap) in a typical realization. We note that one is able to decrease the mode-spacing by enlarging the size of the PC graph, and we choose the current system scale due to limited computational power. One can create a statistical ensemble of chaotic PC graphs by changing the length of the bonds for a given graph topology.

The E-field profile for a particular eigenmode solution of a graph is shown in Fig. 3b. It is clear that the graph mode is localized to the defect waveguide region and displays a longitudinal sinusoidal standing wave pattern. The mode amplitude on a single bond is uniform but varies between different bonds (shown by the color differences), where bonds

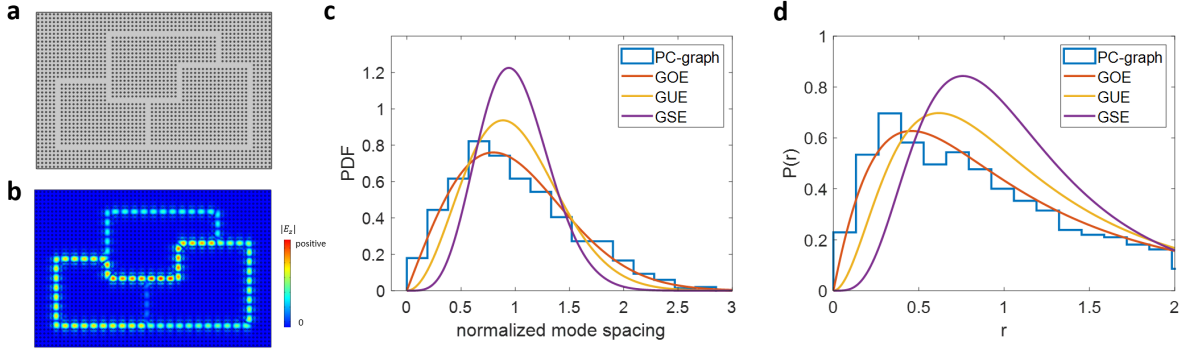


FIG. 3. **a.** Schematic diagram of the PC waveguide graph system. The graph bonds are shown as the clear gray channels and the rectangular lattice is shown as a lattice of dielectric rods (black circles). **b.** The simulated  $|E_z|$  profile of the graph system eigenmode at 2.8GHz. **c** shows the statistics of the normalized mode spacing from graph simulation (histogram). The theoretical predictions for the GOE, GUE and GSE systems are shown in red, yellow and purple curves. **d** shows the statistics of the consecutive mode spacing ratio  $r$  (histogram) and the theoretical predictions for the GOE, GUE and GSE systems.

are defined as straight waveguide regions between 3-way junctions and right-angle bends.

### III. EIGENMODE SPACING STATISTICAL ANALYSIS

We start by conducting the nearest neighbor mode spacing analysis of the proposed PC graphs. An ensemble of 10 different graph realizations are studied numerically and we obtained  $\sim 800$  eigenfrequency values from the ensemble. The graph topology ranges from 13  $\sim$  16 straight segments and 11  $\sim$  14 junctions. We note that such an ensemble of graphs are only used for mode-spacing studies. The graph topology is kept fixed in the eigenfunction studies discussed below. Because the topology and the total length  $L_{tot}$  of each graph realization is different, we normalize the system eigenmodes solutions with following method. We first convert the eigenfrequency data into wavenumbers based on the PC-waveguide PBS (Fig. 1c). The eigenmode wavenumbers are then normalized by fitting to an integrated density of states  $n(k) = c_1 k + c_2 k^{0.5} + c_3$ , where  $c_{1,2,3}$  are fitting parameters [36].

	PC-Graph	GOE	GUE	GSE
$\langle r \rangle$	1.89	1.75	1.37	1.18
$\langle \tilde{r} \rangle$	0.51	0.54	0.60	0.68

TABLE I. The summarized consecutive mode spacing ratios of the photonic crystal graph (PC-Graph) system and the theoretical predictions for the GOE, GUE and GSE systems [42].

Using the fitted  $c_{1,2,3}$  values, we computed the normalized level  $k$  and then obtain the nearest neighbor spacing by  $k_{i+1} - k_i$ , where  $i$  is the index of energy level. The distribution of the normalized mode spacing values of the entire ensemble is shown as the histogram in Fig. 3c. We have also included the theoretical predictions of the mode-spacing statistics for the GOE (Gaussian Orthogonal Ensemble), GUE (Gaussian Unitary Ensemble), and GSE (Gaussian Symplectic Ensemble) in the figure. The three theoretical predictions are based on Random Matrix Theory (RMT) [37–39], which is widely studied as a seminal method of understanding the universal statistical properties of wave-chaotic systems [40, 41]. As shown in Fig. 3c, the distribution of the normalized mode-spacing matches reasonably well with the theoretical prediction for the GOE class. Good agreement between the graph nearest neighbor mode-spacing statistics and the RMT theoretical prediction is also reported in various works on graphs, although long-range statistical quantities tend to show non-universal behaviors due to the trapped-mode problem [3, 24–26].

In addition to the mode-spacing distribution test, we note that the method of consecutive mode spacing ratios  $r_i = \frac{s_i}{s_{i-1}}$  and  $\tilde{r}_i = \min\left(r_i, \frac{1}{r_i}\right)$  can also be adopted [42]. For the PC graphs, the averaged values of  $\langle r \rangle = 1.89$  and  $\langle \tilde{r} \rangle = 0.51$ , which are closer to the GOE theoretical predictions than the GUE and GSE predictions (Table. I). We further present the distribution of mode-spacing ratios  $r$  of the PC graphs and corresponding theoretical predictions of the GOE, GUE and GSE systems in Fig. 3d. The statistics of  $r$  match reasonably well with the GOE prediction.

#### IV. EIGENFUNCTION ANALYSIS

We next study the statistics of the PC graph eigenfunctions. The eigenfunction statistics have been studied experimentally in 2D chaotic systems by probing the electromagnetic (EM) standing wave field inside a microwave cavity [5, 43–47]. In those studies, the experimental probability amplitude distribution and two-point correlation function agree well with the [random plane wave conjecture](#). Here, the wave properties of the entire PC graph (nodes and bonds) can be faithfully simulated. Here we employ the same eigenvalue simulation model used in the mode-spacing studies above. For a graph system, the telegrapher’s equation is formally equivalent to the 1D Schrödinger equation, where the wavefunction  $\psi$  is represented by the wave voltage. For thin parallel plate waveguides, the wave voltage difference between the top and bottom metallic plates is represented by the  $E_z$  value at the middle cutting plane (at the height of  $z = h_0/2$ ). Because the PC graph bonds have a finite width, the bond eigenfunction will be evaluated along a 1D line at the center of the waveguide (shown as the black dashed line in Fig. 1d). We next examine two PC graph eigenfunction characterization methods.

*Method I: grid-wise representation.* For each eigenmode of each graph realization, we will use the entire set of the graph bond  $|E_z|^2$  vs. longitudinal position along the center-line of the waveguide data points to represent the eigenfunction. The name ‘grid-wise’ comes from the granular nature of this method, where the total number of eigenfunction data points is inversely proportional to the computational grid size. We study the wavefunction statistics of the PC graph by computing the distribution of the normalized probability density  $v$ , which is defined as the square of the eigenfunction values  $v_j = |\psi(r_j)|^2 = \frac{|E_z(r_j)|^2 \cdot L_{tot}}{\sum_j |E_z(r_j)|^2 \cdot \Delta L_j}$ , where  $L_{tot}$  is the total length of the graph,  $r_j$  and  $\Delta L_j$  are the location and the grid size of

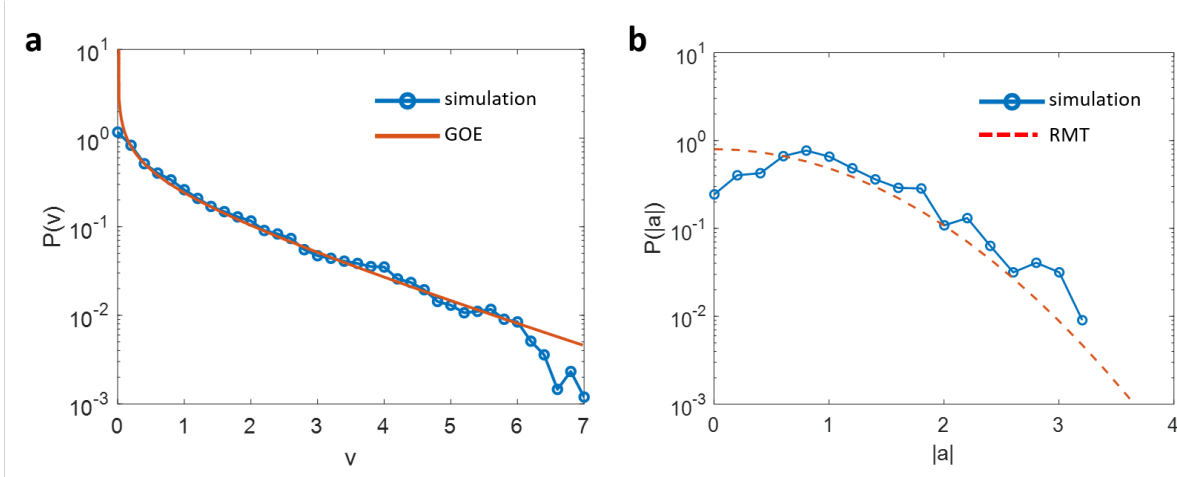


FIG. 4. **a.** Probability amplitude distribution of photonic crystal defect waveguide graph eigenmodes obtained from the grid-wise method (symbols connected by blue line). The theoretical prediction for systems with GOE statistics is in red. **b.** shows the statistics of the normalized bond amplitude value  $|a|$  (symbols connected by blue line) and the Gaussian distribution (red dashed).

the  $j$ 'th grid point,  $|E_z(r_j)|$  is the z-directed electric field magnitude at the  $j$ 'th grid point, and the summation in the denominator runs over every graph grid point. In our simulation, the grid size  $\Delta L_j \sim 0.05\lambda_{op}$  where  $\lambda_{op} = 10\text{cm}$  is the operating wavelength at  $3\text{GHz}$ . The distribution of the probability density values is computed using the data from [all simulated eigenmode solutions \(48 in specific\)](#) for a single realization of the graph, and the results are shown in Fig. 4a, and discussed below.

*Method II: bond-value representation.* For each graph realization, the eigenfunction of a mode is represented by a set of 'bond-values'  $E_z(b_m)$  which is defined as the amplitude of the standing-wave wavefunction on the graph bond  $b_m$ . The quantity  $m$  is the index of the bond and runs from 1 to 14. The standing wave on the bond is made up of two counter propagation waves  $\psi(x) = a_m e^{ikx} + a_m^* e^{-ikx}$ , where  $a_m$  is the wavefunction amplitude at bond  $b_m$  and  $x$  is the distance from a vertex along the bond. We first conduct a sine-fit of the raw  $E_z(x)$  values on each bond, which yields the amplitude, and the value of  $|a_m|$  is obtained as 1/2 of the amplitude value. The normalization process follows the same method

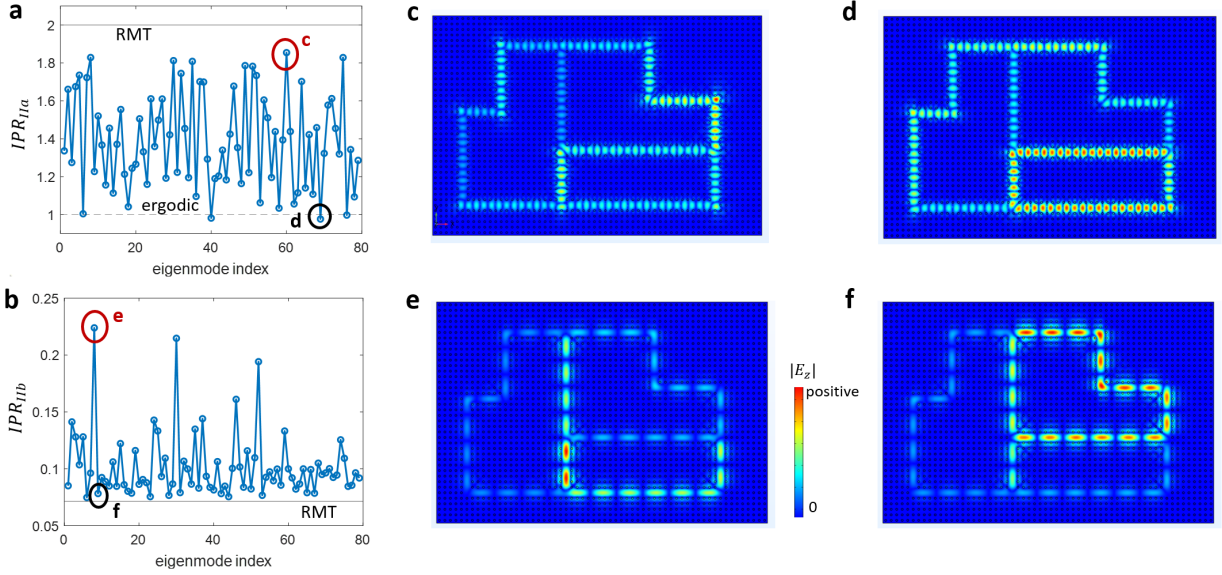


FIG. 5. **a.** The inverse participation ratio (IPR) of graph eigenmodes obtained from the bond-value method, computed based on the method. IIa. The simulated  $|E_z|$  profile of the red (black) circled mode in **a** is shown in **c** (**d**). **b.** The inverse participation ratio (IPR) of graph eigenmodes computed based on the method. II b. The simulated  $|E_z|$  profile of the red (black) circled mode in **b** is shown in **e** (**f**).

as in Ref. [48] which ensures that  $\sum_m L(b_m)|a_m|^2 = L_{tot}$  where  $L(b_m)$  is the length of bond  $b_m$ . Here the distribution of the probability density values is computed over  $14 \times 78$  data points, where 14 is the number of the bonds and 78 is the number of eigenmode solutions from one realization of the graph, and the results for  $P(|a|)$  are shown in Fig. 4b.

We first discuss the eigenfunction statistics obtained using the grid-wise method in Fig. 4a. The theoretical prediction of the GOE systems, given by  $P(x) = \frac{1}{\sqrt{2\pi x}}e^{-x/2}$ , is shown as solid lines. We find that the simulated PC graph result matches reasonably well with the GOE prediction. We notice that a mismatch between the graph data and the GOE prediction exists at the small and large probability density values. One possibility is that this method tends to over-count the appearance of medium-sized eigenfunction values (similar to the systematic errors experienced in Ref. [5]). It may also indicate that the data simply does not match the GOE prediction. In addition to the discrete eigenfunction imaging

method, we note that the eigenfunction statistics may also be tested through resonance width distributions in transmission measurements (Porter-Thomas statistics) [7, 49].

The random plane wave hypothesis underlying RMT eigenfunction treatments [37, 50] predicts that the complex coefficients  $a_m$  should have Gaussian random fluctuations [48, 51]. Here we use *Method II* to study the distribution of the normalized bond-values  $|a|$ , in Fig. 4b, and find some degree of agreement with the random plane-wave prediction. However, a clear deviation from Gaussian statistics is seen for low amplitudes, similar to the deviation observed with *Method I*. Together, these results suggest that the wavefunction statistics of this simple graph are not fully consistent with the random plane wave hypothesis.

We next present the inverse participation ratio (IPR) computation based on the bond-value method (*Method II*) in Fig. 5. IPR is a measure of the degree of localization for a wave function [48, 51], and can be used to quantify the degree of deviation of wavefunction statistics from the random plane wave hypothesis. Based on its IPR value, the eigenfunction behavior varies between two limits, namely the maximum ergodic limit where the wave function occupies each graph bond with equal chance, and the maximum localization limit where the eigenmode is confined to only one bond. RMT predicts an IPR value by assuming Gaussian random fluctuation of the eigenfunctions. Two different IPR definitions are tested here. Method IIa follows the definition in Ref. [48], where the IPR value for each graph mode is evaluated using the formula  $IPR_{IIa} = \langle |a_m|^4 \rangle$ . As shown in Fig. 5a, the IPR values of the photonic crystal graph modes vary erratically but lie between the maximum ergodic limit ( $IPR_{IIa} = 1$ ) and the RMT prediction limit ( $IPR_{IIa} = 2$ ) [48]. In the maximum localization limit the  $IPR_{IIa} = B$ , where  $B = 14$  is the number of graph bonds, and the results are far from this limit. Method IIb follows the definition in Ref. [51] where  $IPR_{IIb} = \sum_m |\tilde{a}_m|^4 / [\sum_m |\tilde{a}_m|^2]^2$ . The quantity  $\tilde{a}_m$  is the un-normalized bond wavefunction

amplitude. Here, the graph IPR values also vary erratically from mode to mode (Fig. 5b), but lie well below the maximum localization limit ( $IPR_{IIb} = 1$ ) and closer to the RMT prediction limit ( $IPR_{IIb} = 1/B = 0.07$ ) [51].

The conclusions we draw from the above two methods are not exactly the same. For Method IIa, two exemplary eigenfunction profiles are shown in Figs. 5c and d, which correspond to the RMT and ergodic limits, respectively. One may directly spot the different nature of these two modes based on their eigenfunction patterns, which is a unique advantage of the photonic crystal graph system. For Method IIb, we present the eigenfunction profile of two neighboring graph modes in Figs. 5e and f. The eigenmode in Fig. 5e has a larger value of  $IPR_{IIb}$  and shows a strongly localized distribution. That in Fig. 5f has a small value of  $IPR_{IIb}$  and is more evenly distributed over the bonds. The average value of IPR over all the modes are more meaningful in this case, and we have  $\langle IPR_{IIa} \rangle = 1.39$  and  $\langle IPR_{IIb} \rangle = 0.10$  which are closer to the ergodic and RMT limits, respectively, than to the localization limit. Previous work [1, 48] on IPR on quantum graphs shows the surprising results that larger graphs, with the number of vertices  $> 10$ , tend to show strong deviations from RMT predictions, while smaller graphs show better agreement.

Taking into account the eigenfunction and IPR statistics, it would appear that PC graphs are close to the random plane wave condition for tetrahedral graphs, but clear systematic differences remain. The complex vertex scattering properties of right-angle bends and T-junctions, along with the unusual  $\omega(k)$  dispersion relation of PC defect waveguide modes, suggest that PC defect graphs may be very effective for future wave chaotic studies.

## V. CONCLUSION

To conclude, we have designed and simulated an alternative chaotic graph system with photonic crystal defect waveguides that show an unusual dispersion relation. We show that a series of statistical studies can be carried out on closed graphs, including nearest-neighbor spacing statistics and eigenfunction statistics studies. Because both the graph bonds and nodes can be probed directly, one may better analyze the non-universal features of chaotic graphs using a PC system. We note that the PC 3-way and right-angle junctions have complicated scattering properties, and it is possible to adjust the degree of localization by engineering the scattering properties of the PC waveguide junctions. These properties of the PC waveguides may facilitate further studies of localization phenomena in graphs, for example the emergence or suppression, and the further manipulation, of trapped modes.

## ACKNOWLEDGEMENTS

This work was supported by ONR under Grant No. N000141912481, AFOSR COE Grant FA9550-15-1-0171, and the Maryland Quantum Materials Center.

---

\* [skma@umd.edu](mailto:skma@umd.edu)

- [1] O. Hul, S. Bauch, P. Pakoński, N. Savytsky, K. Życzkowski, and L. Sirko, *Physical Review E* **69**, 056205 (2004).
- [2] A. Rehemangiang, M. Richter, U. Kuhl, and H.-J. Stöckmann, *Physical Review Letters* **124**, 116801 (2020).
- [3] J. Lu, J. Che, X. Zhang, and B. Dietz, *Physical Review E* **102**, 022309 (2020).
- [4] L. Chen, T. Kottos, and S. M. Anlage, *Nature Communications* **11**, 5826 (2020).
- [5] D. H. Wu, J. S. A. Bridgewater, A. Gokirmak, and S. M. Anlage, *Physical Review Letters*

- 81**, 2890 (1998).
- [6] C. Dembowski, B. Dietz, H.-D. Gräf, A. Heine, F. Leyvraz, M. Miski-Oglu, A. Richter, and T. H. Seligman, *Physical Review Letters* **90**, 014102 (2003).
- [7] C. Dembowski, B. Dietz, T. Friedrich, H.-D. Gräf, H. L. Harney, A. Heine, M. Miski-Oglu, and A. Richter, *Physical Review E* **71**, 046202 (2005).
- [8] S. Hemmady, X. Zheng, E. Ott, T. M. Antonsen, and S. M. Anlage, *Physical Review Letters* **94**, 014102 (2005).
- [9] U. Kuhl, R. Höhmann, J. Main, and H.-J. Stöckmann, *Physical Review Letters* **100**, 254101 (2008).
- [10] S. Shinohara, T. Harayama, T. Fukushima, M. Hentschel, T. Sasaki, and E. E. Narimanov, *Physical Review Letters* **104**, 163902 (2010).
- [11] B. Dietz and A. Richter, *Physica Scripta* **94**, 014002 (2019).
- [12] S. Hemmady, T. M. Antonsen, E. Ott, and S. M. Anlage, *IEEE Transactions on Electromagnetic Compatibility* **54**, 758 (2012).
- [13] B. Xiao, T. M. Antonsen, E. Ott, Z. B. Drikas, J. G. Gil, and S. M. Anlage, *Physical Review E* **97**, 062220 (2018).
- [14] S. Ma, B. Xiao, R. Hong, B. Addissie, Z. Drikas, T. Antonsen, E. Ott, and S. Anlage, *Acta Physica Polonica A* **136**, 757 (2019).
- [15] S. Ma, B. Xiao, Z. Drikas, B. Addissie, R. Hong, T. M. Antonsen, E. Ott, and S. M. Anlage, *Physical Review E* **101**, 022201 (2020).
- [16] S. Ma, S. Phang, Z. Drikas, B. Addissie, R. Hong, V. Blakaj, G. Gradoni, G. Tanner, T. M. Antonsen, E. Ott, and S. M. Anlage, *Physical Review Applied* **14**, 14022 (2020).
- [17] B. W. Frazier, T. M. Antonsen, S. M. Anlage, and E. Ott, *Physical Review Research* **2**, 043422 (2020).
- [18] X. Zheng, S. Hemmady, T. M. Antonsen, S. M. Anlage, and E. Ott, *Physical Review E* **73**, 046208 (2006).
- [19] J. A. Hart, T. M. Antonsen, and E. Ott, *Physical Review E* **80**, 041109 (2009).
- [20] J.-H. Yeh, J. A. Hart, E. Bradshaw, T. M. Antonsen, E. Ott, and S. M. Anlage, *Physical Review E* **82**, 041114 (2010).
- [21] X. Li, C. Meng, Y. Liu, E. Schamiloglu, and S. D. Hemmady, *IEEE Transactions on Electromagnetic Compatibility* **57**, 448 (2015).

- [22] Y. Aurégan and V. Pagneux, *Acta Acustica united with Acustica* **102**, 869 (2016).
- [23] M. Zhou, E. Ott, T. M. Antonsen, and S. M. Anlage, *Chaos: An Interdisciplinary Journal of Nonlinear Science* **29**, 033113 (2019).
- [24] M. Białous, V. Yunko, S. Bauch, M. Lawniczak, B. Dietz, and L. Sirko, *Physical Review Letters* **117**, 144101 (2016).
- [25] B. Dietz, V. Yunko, M. Białous, S. Bauch, M. Lawniczak, and L. Sirko, *Physical Review E* **95**, 052202 (2017).
- [26] J. Che, J. Lu, X. Zhang, B. Dietz, and G. Chai, *Physical Review E* **103**, 042212 (2021).
- [27] J. D. Joannopoulos, P. R. Villeneuve, and S. Fan, *Nature* **386**, 143 (1997).
- [28] J. D. Joannopoulos, S. G. Johnson, J. N. Winn, and R. D. Meade, *Photonic Crystals* (Princeton University Press, 2008).
- [29] B. Xiao, K. Lai, Y. Yu, T. Ma, G. Shvets, and S. M. Anlage, *Physical Review B* **94**, 195427 (2016).
- [30] K. Lai, T. Ma, X. Bo, S. Anlage, and G. Shvets, *Scientific Reports* **6**, 28453 (2016), 1601.01311.
- [31] S. Ma, B. Xiao, Y. Yu, K. Lai, G. Shvets, and S. M. Anlage, *Physical Review B* **100**, 085118 (2019).
- [32] S. Ma and S. M. Anlage, *Applied Physics Letters* **116**, 250502 (2020).
- [33] Y. G. N. Liu, P. S. Jung, M. Parto, D. N. Christodoulides, and M. Khajavikhan, *Nature Physics* **17**, 704 (2021).
- [34] W. Maimaiti, B. Dietz, and A. Andreanov, *Physical Review B* **102**, 214301 (2020).
- [35] A. Mekis, J. C. Chen, I. Kurland, S. Fan, P. R. Villeneuve, and J. D. Joannopoulos, *Physical Review Letters* **77**, 3787 (1996).
- [36] A. Rehemangiang, M. Allgaier, C. H. Joyner, S. Müller, M. Sieber, U. Kuhl, and H.-J. Stöckmann, *Physical Review Letters* **117**, 064101 (2016).
- [37] M. V. Berry, *European Journal of Physics* **2**, 91 (1981).
- [38] T. Kottos and U. Smilansky, *Physical Review Letters* **79**, 4794 (1997).
- [39] T. Kottos and U. Smilansky, *Annals of Physics* **274**, 76 (1999).
- [40] G. Casati, F. Valz-Gris, and I. Guarneri, *Lettere al Nuovo Cimento* **28**, 279 (1980).
- [41] O. Bohigas, M. J. Giannoni, and C. Schmit, *Physical Review Letters* **52**, 1 (1984).
- [42] Y. Y. Atas, E. Bogomolny, O. Giraud, and G. Roux, *Physical Review Letters* **110**, 084101 (2013).

- [43] A. Kudrolli, V. Kidambi, and S. Sridhar, *Physical Review Letters* **75**, 822 (1995).
- [44] A. Gokirmak, D.-H. Wu, J. S. A. Bridgewater, and S. M. Anlage, *Review of Scientific Instruments* **69**, 3410 (1998).
- [45] S.-H. Chung, A. Gokirmak, D.-H. Wu, J. S. A. Bridgewater, E. Ott, T. M. Antonsen, and S. M. Anlage, *Physical Review Letters* **85**, 2482 (2000).
- [46] U. Kuhl, E. Persson, M. Barth, and H.-J. Stöckmann, *The European Physical Journal B* **17**, 253 (2000).
- [47] Y. Hlushchuk, L. Sirko, U. Kuhl, M. Barth, and H.-J. Stöckmann, *Physical Review E* **63**, 046208 (2001).
- [48] L. Kaplan, *Physical Review E* **64**, 036225 (2001).
- [49] H. Alt, H. D. Gräf, H. L. Harney, R. Hofferbert, H. Lengeler, A. Richter, P. Schardt, and H. A. Weidenmüller, *Physical Review Letters* **74**, 62 (1995).
- [50] P. O'Connor, J. Gehlen, and E. J. Heller, *Physical Review Letters* **58**, 1296 (1987).
- [51] O. Hul, P. Šeba, and L. Sirko, *Physical Review E* **79**, 066204 (2009).